

## Three- and four- $\mu\text{m}$ -thick $\text{YBa}_2\text{Cu}_3\text{O}_7$ layers with high critical-current densities on flexible metallic substrates by the $\text{BaF}_2$ process

Vyacheslav F. Solovyov,<sup>a)</sup> Harold J. Wiesmann, Qiang Li, David O. Welch, and Masaki Suenaga

Materials Science Department, Brookhaven National Laboratory, 76 Cornell Avenue, Upton, New York 11973

(Received 8 July 2005; accepted 14 November 2005; published online 4 January 2006)

We report on the synthesis and performance of 3- and 4- $\mu\text{m}$ -thick  $\text{YBa}_2\text{Cu}_3\text{O}_7$  films on buffered metallic tapes. The precursor films were deposited by vacuum coevaporation of  $\text{BaF}_2$ , Y, and Cu on the substrates and converted to  $\text{YBa}_2\text{Cu}_3\text{O}_7$  by the  $\text{BaF}_2$  *ex situ* process at reduced processing gas pressures. The best value of critical-current density  $J_c$  for these films was  $\sim 3.8 \times 10^3$  A/mm<sup>2</sup> at 77 K and in 1 T external magnetic field perpendicular to the film plane. Also, estimated critical-current densities per width of tape  $J_{cw}$  at zero magnetic field were  $\sim 60$  and  $\sim 80$  A/mm for 3- and 4- $\mu\text{m}$ -thick films, respectively. In order to achieve these high- $J_c$  values, the films were processed at high growth rates ( $\sim 0.7$  nm/s) and the oxygen partial pressure  $p(\text{O}_2)$  was varied to minimize the growth of the “granular” *c* axis and randomly oriented  $\text{YBa}_2\text{Cu}_3\text{O}_7$  grains. A simple thermodynamic argument is also given to describe the observed dependence of the nucleation of  $\text{YBa}_2\text{Cu}_3\text{O}_7$  with different orientations on  $p(\text{O}_2)$ . This result demonstrates the feasibility of fabricating coated conductors with a single  $\text{YBa}_2\text{Cu}_3\text{O}_7$  layer having the critical current of the order of 100 A/mm at self-field and liquid-N<sub>2</sub> temperature. © 2006 American Institute of Physics. [DOI: 10.1063/1.2150590]

### I. INTRODUCTION

The success of the  $\text{YBa}_2\text{Cu}_3\text{O}_7$ - (YBCO) coated conductor technology for electric-power applications heavily relies on the availability of long wires with high critical currents. For example, the goals set by the US Department of Energy for critical currents per width of tape  $J_{cw}$  are (1) 30 A/mm (self-field critical currents at 77 K) for 300-m-long tapes by 2006 and (2) 100 A/mm for 1000 m tapes by 2010.<sup>1</sup> The first goal has been met for some short specimens, and the manufacturers are currently working to reproduce these high critical currents in long lengths. However, the second goal for  $J_{cw}$  is very far from being met, even in short lengths, except for one special case, which will be discussed below. Since achieving the critical currents beyond the 30 A/mm level becomes difficult even for short specimens, a thorough investigation of the means to achieve such high critical currents is required to assist the manufacturers to reach the second DOE goal by 2010. One possible approach to achieve these high critical currents is to increase the thickness ( $\geq 1$   $\mu\text{m}$ ) of the YBCO films. However, in the past, degradation in critical-current densities  $J_c$  with thickness has appeared to be universal for all popular methods of YBCO growth, e.g., pulsed laser deposition (PLD) methods<sup>2</sup> and the  $\text{BaF}_2$  process.<sup>3</sup> In fact, it was argued theoretically that the decreases in  $J_c$  of uniform YBCO films with the increasing thickness were intrinsic to the properties of YBCO films and were related to the two-dimensional (2D) to three-dimensional (3D) transition in the nature of flux pinning in these films.<sup>4</sup> So far, the only technique for achieving very high  $J_c$  in thick (e.g.,  $> 3$   $\mu\text{m}$ ) films has involved making

multilayers of YBCO ( $< 1$   $\mu\text{m}$ ) and  $\text{CeO}_2$  ( $\sim 50$  nm) films by PLD.<sup>5</sup> This is, in essence, replacing a thick film with a stack of thinner but high- $J_c$  films. In one case, a value of  $J_{cw}$  as high as 140 A/mm in width was reported for a 3.5- $\mu\text{m}$ -thick film. These results are very impressive. However, it is also important to investigate whether it is possible to produce the films with similarly high  $J_{cw}$  using other YBCO synthesis approaches, which are suitable for large-scale fabrication of YBCO tapes. Recently, using the  $\text{BaF}_2$  process, Feenstra *et al.* were able to grow YBCO films whose  $J_c$  values were thickness independent and were  $\sim 2.5 \times 10^4$  A/mm<sup>2</sup> at self-field and 77 K.<sup>6</sup> This was accomplished by increasing the growth rate of YBCO layers up to  $\sim 1.2$  nm/s from the value of  $\sim 0.2$  nm/s which was often used. Unfortunately, the synthesis of the films with this value of  $J_c$  was only possible for thickness up to  $\sim 1.6$   $\mu\text{m}$ . Beyond this thickness,  $J_c$  of the films was drastically decreased due to the microstructural degradation of YBCO layers. Thus, the values of  $J_{cw}$  were limited to  $\sim 35$  A/mm for these films.

We have also investigated the making of thick YBCO layers by the  $\text{BaF}_2$  process and have analyzed the factors which contribute to the attainment of high  $J_c$  in thick ( $\geq 1$   $\mu\text{m}$ ) YBCO layers on single-crystalline  $\text{SrTiO}_3$  (Refs. 7 and 8) and buffered metallic substrates.<sup>9,10</sup> It was found that the initial formation of *c*-axis-oriented nuclei was very important, since the texture of the films was essentially determined by the orientation of the nuclei, which depended strongly on the permeability of the reaction gases through the precursor films.<sup>7-9</sup> In our most recent study<sup>10</sup> we have grown *c*-axis-oriented 2- $\mu\text{m}$ -thick films on  $\text{CeO}_2$ -buffered metal tapes using atmospheric-pressure processing. However, de-

<sup>a)</sup>Electronic mail: solov@bnl.gov

spite the good texture,  $J_c$  of these films never exceeded  $0.5 \times 10^4$  A/mm<sup>2</sup> in zero field at 77 K. In general, the morphology of these YBCO films could be described as a mosaic of very large ( $>10$   $\mu\text{m}$ ) *c*-axis-oriented grains. Such “granular” YBCO films were formed from very low densities of the nuclei, i.e., the internuclei distances were much greater than the film thickness. In such cases, the nuclei grew to the surface before they merged with neighboring nuclei, and then grew laterally to cover the entire film surface. We speculated that poor connectivity between such oversized grains is responsible for low  $J_c$ , although the exact reason is yet to be found. We noted that  $J_c$  improved as the grains became smaller just prior to the formation of dense randomly oriented platelets. In addition, we observed in this study that there was a trend of decreasing YBCO grain sizes with decreasing water vapor partial pressure  $p(\text{H}_2\text{O})$  and increasing oxygen partial pressure  $p(\text{O}_2)$ .

This finding led us to conclude that increasing the nuclei density by fast growth processing at low  $p(\text{H}_2\text{O})$  was a promising strategy for achieving high  $J_c$  in multimicrometer-thick films.<sup>10</sup> As we have shown earlier, one way to achieve high rates of conversion is by reducing process-gas pressure.<sup>11–15</sup> This method also allowed us to process the films at substantially lower  $p(\text{H}_2\text{O})$ . In this article, we report that it is possible to synthesize 3- and 4- $\mu\text{m}$ -thick YBCO films with high current densities on CeO<sub>2</sub>-buffered metallic substrates by the use of the subatmospheric-pressure processing schemes previously described in Ref. 11.

## II. EXPERIMENTAL PROCEDURE

Vacuum coevaporation of Y, BaF<sub>2</sub>, and Cu was used for the deposition of the precursor layers. The deposition setup and a typical protocol for *ex situ* heat treatment to form YBCO were described earlier.<sup>11,16</sup> Fluorinated precursor layers were deposited at an effective rate of 10 nm/s on buffered metallic substrates at the ambient temperature. The substrates were provided by American Superconductor Corporation (Westborough, MA). They were textured Ni–W alloy tapes (RABITS™), which were buffered with the following oxide layers in sequence: (Ni–W)–75 nm Y<sub>2</sub>O<sub>3</sub>–75 nm YSZ (yttria-stabilized zirconia)–75 nm CeO<sub>2</sub>. The substrates used in this study were  $3 \times 10$  mm<sup>2</sup> coupons cut from 10-mm-wide tapes. Inspection of as-deposited films by scanning electron microscopy showed that the precursor layers were dense and there was a negligible volume change after their conversion to YBCO. The layers were also mechanically robust, with neither signs of cracking nor delamination even when they were as thick as 4  $\mu\text{m}$ .

For the present study, the heat treatment for the YBCO formation was carried out at a temperature of 735 °C and at a total processing gas pressure of  $\sim 21$  Torr. The gas was composed of nitrogen at  $\sim 20$  Torr, water vapor at 0.5 Torr, and oxygen which was varied between 40 and 300 mTorr. The composition of the processing atmosphere was confirmed with a quadrupole mass spectrometer attached to the system. This was especially important, since the YBCO nuclei densities on CeO<sub>2</sub> were previously found to be very sensitive to  $p(\text{O}_2)$ ,<sup>10</sup> although the changes in  $p(\text{O}_2)$  of the

processing gas hardly influenced the growth rates for the films grown on SrTiO<sub>3</sub> with the processing gas at atmospheric pressure.<sup>17</sup>

In order to determine the growth rate of YBCO films in this process, we recorded the electrical conductivity of the films *in situ* during the reaction process.<sup>17</sup> When we noted a plateau of the conductivity versus time plot, we took it as a sign of the YBCO conversion completion, and the growth rates were calculated from these data. Under the present reaction condition, YBCO on  $3 \times 10$  mm<sup>2</sup> substrates grew at an approximate rate of 0.7 nm/s. In addition, in order to observe the effect of lowered growth rates on  $J_c$  at an identical reaction gas composition, we restricted the reaction gas flow around the specimen by surrounding it with a quartz baffle. This reduced the rate of extracting HF from the specimen and reduced the YBCO growth rate down to  $\sim 0.2$  nm/s.<sup>18</sup>

Another important processing step in this study was heat treatment of the precursor films in water vapor at low temperatures ( $\sim 400$  °C) prior to the high-temperature treatment for the YBCO formation. All of the specimens were pretreated under the same conditions. At present, we do not fully understand how this pretreatment of the precursor affects the nucleation of YBCO. We believe that this process helps us to improve the HF permeability of the precursor films, and we find that this is a necessary step in making high- $J_c$  specimens on CeO<sub>2</sub>-buffered substrates. The effects of this treatment on the physical properties of the precursors are under investigation and will be discussed at a later date.

Transport measurements of the critical currents  $I_c$  of the specimens were performed in liquid N<sub>2</sub> using a four-probe technique.  $E=0.1$   $\mu\text{V}/\text{mm}$  was used as the voltage criterion for  $I_c$ . An iron electromagnet, which was immersed in liquid N<sub>2</sub>, supplied an external dc magnetic field with values up to 1 T. Current contacts for our specimens ( $3 \times 10$  mm<sup>2</sup>) typically held up to 50–60 A of dc is before the contacts and the specimen disintegrated. This made measurements of self-field  $I_c$  difficult for high- $J_c$  specimens. Therefore, unless specifically stated, all of the reported  $J_c$  data were determined at 77 K and 1 T. Magnetic field was always applied perpendicular to the face of the specimen.

## III. RESULTS

Figure 1 shows the variation of  $J_c$  as a function of  $p(\text{O}_2)$  in the processing atmosphere for YBCO growth rates of 0.7 and 0.2 nm/s for 3- $\mu\text{m}$ -thick films and of 0.7 nm/s for 4- $\mu\text{m}$ -thick films. The highest  $J_c$  at 1 T and 77 K was  $\sim 3.8 \times 10^3$  A/mm<sup>2</sup> for both 3- and 4- $\mu\text{m}$ -thick films when their growth rates were at  $\sim 0.7$  nm/s. In order to estimate the zero-field values of  $J_c$  of these films, we used the ratio  $J_c(0 \text{ T})/J_c(1 \text{ T})=5$  since this factor is known to vary from 4 to 6 for similarly processed YBCO films. Using this ratio, we estimated the highest zero-field  $J_c$  for these specimens to be approximately  $2 \times 10^4$  A/mm<sup>2</sup>. This translates to critical-current densities  $J_{c0}$  of  $\sim 60$  and  $\sim 80$  A/mm for 3- and 4- $\mu\text{m}$ -thick specimens, respectively. In order to confirm these estimates, we used focused laser beam to cut a 0.24-mm-wide bridge on one of the 3- $\mu\text{m}$ -thick specimens with

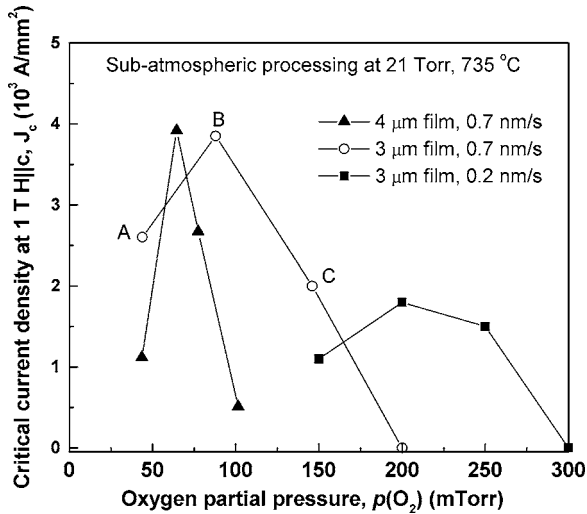


FIG. 1. Critical-current density of 3- and 4- $\mu\text{m}$ -thick YBCO films as a function of the partial pressure of oxygen,  $p(\text{O}_2)$ . The samples were processed at  $T=735^\circ\text{C}$ ,  $p(\text{H}_2\text{O})=0.5$  Torr, and the total process-gas pressure of 21 Torr with the balance of the process gas being  $\text{N}_2$ . Two film growth rates, 0.7 and 0.2 nm/s, were used for 3- $\mu\text{m}$ -thick specimens while 4- $\mu\text{m}$ -thick films were grown at 0.7 nm/s.

$J_c(1\text{ T})=3.8 \times 10^3 \text{ A/mm}^2$ , and obtained  $J_c$  by direct transport measurement to be  $2.3 \times 10^4 \text{ A/mm}^2$  for its self-field critical-current density. This is in reasonable agreement with our estimates of self-field  $J_c$  above. The slight discrepancy in  $J_c$  (self-field) between the estimated and directly measured values is likely to be due to the nonuniformity in  $J_c$  across the specimen.

The values of  $J_c(1\text{ T})$  have maxima with respect to the variation of  $p(\text{O}_2)$  in the processing gas, as shown in Fig. 1. The  $p(\text{O}_2)$  corresponding to the maximum of  $J_c$  was shifted toward lower  $p(\text{O}_2)$ , and the peak narrowed as the film thickness increased from 3 to 4  $\mu\text{m}$ . Also, the slower growth rate resulted in  $J_c$  peaking at a higher  $p(\text{O}_2)$  with a wider peak than those for the specimens processed at higher growth rates. Unfortunately, the values of  $J_c$  for these specimens were invariably lower.

Observation of the specimen surfaces by optical microscopy helped us to reveal microstructural differences associated with the variations in  $J_c$  with  $p(\text{O}_2)$  in Fig. 1. Optical micrographs of the surfaces of 3- $\mu\text{m}$ -thick specimens are shown in Figs. 2(a)–2(c). These correspond to the specimens for which  $J_c$  data points which are labeled A, B, and C in

Fig. 1. The optical image in Fig. 2(c) shows a large density of rodlike features on the film surface. These were found to be YBCO platelets. From x-ray-diffraction data, most of these appear to have (103,013) planes parallel to the substrate surface but were without strong in-plane alignment. (However, we cannot state the orientations of these platelets with certainty, and some of the platelets are likely to be oriented in the directions other than [103,013] since the strongest line intensity for YBCO powder diffraction belongs to this line. But, for simplicity, we will call these [103,013] platelets in the discussion below.) As expected, these platelets, when present in large numbers, reduced the useful cross sections of the YBCO films for the passage of current and thus decreased the overall  $J_c$ . This is an acute problem in thick films since [103,013] grains grow, on average, to lengths of about ten times the film thickness due to the approximately ten-fold anisotropy in YBCO growth rates along the  $ab$  plane compared to the  $c$  axis of YBCO. Interestingly,  $a$ -axis-oriented platelets were hardly observed in this study.

Reducing  $p(\text{O}_2)$  helped us to eliminate most of the [103,013] platelets, as shown in Fig. 2(b), which was the optimum specimen for  $J_c$  among 3- $\mu\text{m}$ -thick films. The sample had a uniform and shiny surface and was practically devoid of [103,013] platelets. After further reduction of  $p(\text{O}_2)$ , [103,013] platelets were completely eliminated, as shown in Fig. 2(a). However, the film surface took a characteristic cobblestone appearance or “granular texture,” and  $J_c$  of the films decreased. From our previous study,<sup>10</sup> we associate this kind of surface texture with film growth from low densities of  $c$ -axis nuclei at the initial stages of the reaction process. As mentioned above, when the  $c$ -axis nuclei were sparsely spaced, YBCO layers were formed by lateral growth after they grew to the surface rather than by vertical growth after the high-density nuclei were joined laterally first.<sup>19</sup> For yet unknown reasons, these films tended to exhibit low  $J_c$ , even though the films were nearly completely  $c$ -axis textured. Thus, very high  $J_c$  films can be synthesized when the growth of [103,013] platelets is minimized while the nucleation of the  $c$ -axis grains is still high. However, we could not simultaneously eliminate granularity and [103,013] grains for the specimens when YBCO films were processed at a slow growth rate,  $\sim 0.2$  nm/s. This explains why lower- $J_c$  values were observed for these specimens, as shown in Fig. 1.

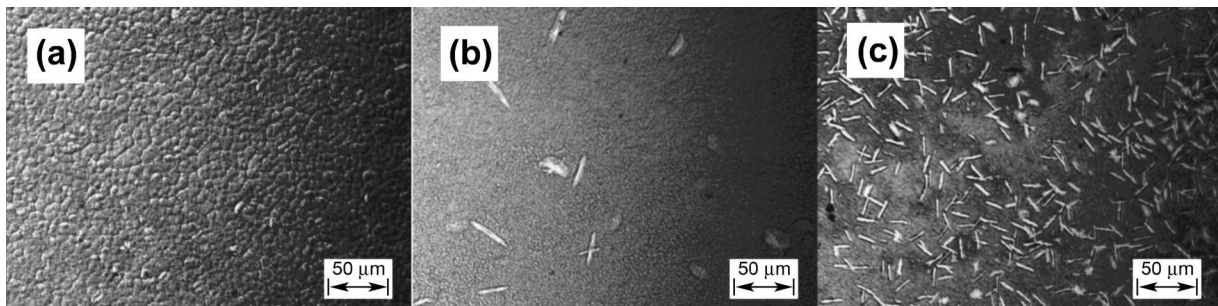


FIG. 2. Optical micrographs, (a), (b), and (c), are from the surfaces of as-prepared 3- $\mu\text{m}$ -thick specimens which were processed at  $p(\text{O}_2)=45, 90,$  and 150 mTorr, respectively, and at  $T=735^\circ\text{C}$ ,  $p(\text{H}_2\text{O})=0.5$  Torr, and the total process-gas pressure of 21 Torr with the balance of the process gas being  $\text{N}_2$ . Also, these specimens correspond to those data which are labeled A, B, and C in Fig. 1.

#### IV. DISCUSSION

In our  $J_c$  optimization effort discussed above, our objective was (1) to minimize the number of [103,013] YBCO platelets while (2) maximizing the density of the  $c$ -axis nuclei to avoid “granular” YBCO grains, i.e., large grains with a cobblestone appearance of the surface. When both of granularity and [103,013] grains were minimized by varying  $p(\text{O}_2)$  for each thickness of YBCO, the values of  $J_c$  were maximized. In order to develop a qualitative understanding of the formation of these grains, we examine a simple thermodynamic argument for the epitaxial formation of YBCO nuclei on a lattice-matched substrate.

The nucleation of YBCO is possible if the precursor/substrate system gains sufficient free energy by the formation of the nuclei at the interface. The Gibbs free energy of a nucleus is a sum of the positive surface  $G^s$  and the negative volume  $G^v$  energies, and the gain in the free energy  $\Delta G$  per unit volume in forming an YBCO nucleus from the precursor on the substrate is given by<sup>20</sup>

$$\Delta G = \Delta(G^s + G^v) = \sigma r^2 + \delta\mu \frac{\gamma r^3}{V}, \quad (1)$$

where  $V$  is the unit-cell volume of YBCO,  $\sigma$  and  $\delta\mu$  are the changes in the effective surface energy per unit area and the volume free energy per mole, respectively, when the precursor phases change to YBCO on a substrate, and  $\gamma$  is the ratio of the height to the radius of the nucleus which is assumed to be a circular disk. The main contribution to  $\sigma$  is the formation of the faces of the disk, the destruction of precursor/substrate interface, and the creation of precursor/YBCO/substrate interfaces. Note that  $\sigma$  is an effective surface energy made up of a weighted average of the various interfacial energy changes, which accompany the formation of the circular disk-shaped nucleus. For simplicity, we use single interface energy (“surface” energy) in our discussion. The nucleation theory predicts that only embryos which are larger than the critical size  $r^*$ , i.e., those which gained sufficient energy, the critical Gibbs free energy  $\Delta G^*$ , can grow to be stable nuclei. Then, omitting nonessential numerical factors, we obtain  $\Delta G^*$  and  $r^*$  for a nucleus as

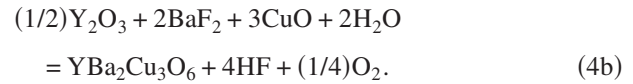
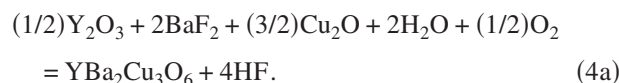
$$\Delta G^* \approx \sigma^3 \left( \frac{V}{\gamma \delta\mu} \right)^2 \text{ and } r^* \approx - \frac{\sigma V}{\gamma \delta\mu}. \quad (2)$$

Also, the nucleation rate  $dN/dt$ ,  $N$  is the number of stable nuclei on the substrate surface per unit area and  $t$  is time, is given by

$$\frac{dN}{dt} \cong \frac{dN_0}{dt} e^{-\Delta G^*/kT}, \quad (3)$$

where  $(dN_0/dt)$  is the nucleation rate with a negligible nucleation barrier,  $\Delta G^* \sim 0$ .<sup>21</sup>

In order to derive the expression for the volumetric free-energy change (or the thermodynamic driving potential),  $\delta\mu$ , for the formation of the YBCO nuclei, we consider the following two formal chemical reactions in the  $\text{BaF}_2$  process:



These represent the two extremes of the possible oxidation states of Cu oxides at the precursor/substrate interface or the reaction front. Equation (4b) is often used, since the reaction condition has been generally thought to be slightly on the CuO side of the line separating the stability of CuO and  $\text{Cu}_2\text{O}$  in the  $\text{O}_2$  partial pressure versus  $1/T$  phase stability diagram for the Cu–O system.<sup>22</sup> However, copper in the precursor has been observed to exist only as  $\text{Cu}_2\text{O}$  adjacent to the interface at the time of nucleus formation, as well as during the early stages of the YBCO growth of a 3- $\mu\text{m}$ -thick film, when the reaction took place at 735 °C and 100 mTorr of  $\text{O}_2$ .<sup>19</sup> Furthermore, it is physically more reasonable to expect the  $\text{O}_2$  term on the left-hand side, rather than that on the right, of the equation since the  $\text{BaF}_2$  process requires  $\text{O}_2$  in the process gas in order to form YBCO. Thus, we use the chemical reaction, Eq. (4a), in the following discussion. In this case, thermodynamic potential  $\delta\mu$  for the reaction is given by

$$\delta\mu = kT \left[ 4 \ln \frac{p(\text{HF})}{p(\text{HF})_e} - 2 \ln \frac{p(\text{H}_2\text{O})}{p(\text{H}_2\text{O})_e} - 0.5 \ln \frac{p(\text{O}_2)}{p(\text{O}_2)_e} \right], \quad (5)$$

where the subscript  $e$  represents the equilibrium partial pressures for the gases. In this expression for the chemical driving potential, the contribution from the  $\text{O}_2$  term is probably very small compared to the other two terms. However, we consider only the last term in the above equation for the discussion of the morphological changes of the YBCO films in Fig. 2 since  $p(\text{O}_2)$  was the only controllable variable in these experiments,  $p(\text{H}_2\text{O})$  being held constant and  $p(\text{HF})$  being unknown.

In the above discussion, we assumed that the processing gases were near equilibrium at the surface of the nucleus and also at the precursor surface in Eq. (4a). These assumptions are probably very good when the films are thin enough for the nearly free diffusion of the reactant gases through the precursor.<sup>18</sup> Although this may not be strictly valid for the thick precursor films being considered here, we will proceed from these assumptions for the purpose of gaining a qualitative understanding of the changes in the surface morphology with  $p(\text{O}_2)$  in the thick films of YBCO which were observed in Fig. 2.

Another variable in Eq. (1) is the effective surface energy  $\sigma$  and in the present case, this is primarily controlled by the degree of the lattice match between YBCO and the substrate  $\text{CeO}_2$ . The lattice parameter of the basal plane of  $\text{YBa}_2\text{Cu}_3\text{O}_{6+\delta}$  for  $\delta \sim 0$  is  $a_{(100)} \sim 0.386$  nm and  $a_{(110)} = \sqrt{2}a_{(100)} \sim 0.542$  nm. That for  $\text{CeO}_2$ , which is cubic, is  $a_{\text{CeO}_2} \sim 0.541$  nm. Hence,  $a_{(110)}$  of  $c$ -axis-oriented YBCO fits very well with  $a_{\text{CeO}_2}$  for the epitaxial growth of YBCO on  $\text{CeO}_2$ . On the other hand, the parameter of the (103,013) planes is  $a_{(103)} \sim 0.556$  nm using the  $c$ -axis lattice constant to be  $\sim 1.182$  nm for YBCO with  $\delta \sim 0$ .<sup>23</sup> The fit of  $a_{(103)}$  with  $\text{CeO}_2$  is reasonably good but not as good as that for the basal planes. Thus, we expect that the effective interfacial energy

for *c*-axis-oriented YBCO,  $\sigma_{(001)}$ , is smaller than  $\sigma_{(103)}$  for the [103,013]-oriented nucleus. Then, it follows from Eq. (2) that the critical Gibbs free energies for the *c*-axis nucleus  $\Delta G^*_{(001)}$  will be less than that for the [103, 013] nucleus  $\Delta G^*_{(103)}$  at a given  $p(\text{O}_2)$ . Thus, the nucleation rates for the *c*-axis nuclei are always greater than those for the [103,013] nuclei.

Now, we discuss the variations in the microstructures of the YBCO films in Fig. 2 with the variations in oxygen partial pressures  $p(\text{O}_2)$  in terms of Eqs. (2), (3), and (5). When  $p(\text{O}_2)$  is very low, the value of  $\Delta G^*_{(001)}$  will be relatively large since the absolute value of  $\delta\mu$  will be small from Eqs. (2) and (5). Then, the nucleation rate  $dN_{(001)}/dt$  and, hence, the initial nuclei density  $N_{(001)}$  for the *c*-axis nuclei will be low. As stated above, under such a condition, we expect a “granular” YBCO surface, as shown in Fig. 2(a). As  $p(\text{O}_2)$  increases, the nucleation rate increases since  $\Delta G^*_{(001)}$  decreases due to the increase of the  $\delta\mu^2$  term. When the density of nuclei  $N_{(001)}$  is sufficiently increased by high  $p(\text{O}_2)$  value, e.g., 90 mTorr, the nuclei grow laterally to merge with the neighboring ones to form a thin YBCO layer and then grow vertically to the surface to form a smooth surface, as shown in Fig. 2(b). At this point, the nucleation rate  $dN_{(103)}/dt$  for the [103,013] platelets is also elevated, but is still low since  $\Delta G^*_{(103)} > \Delta G^*_{(001)}$ . However, the rate is sufficiently large to nucleate a few of them, as can also be seen in Fig. 2(b). When  $p(\text{O}_2)$  is further increased, both of  $\Delta G^*_{(103)}$  and of  $\Delta G^*_{(001)}$  are reduced and thus the nucleation rates for the both types of the nuclei are higher. Although  $dN_{(103)}/dt$  is still smaller than  $dN_{(001)}/dt$ , the absolute value becomes sufficiently large such that a significant number of the [103,013] platelets can be formed among a high density of the *c*-axis grains. This is observed in Fig. 2(c) for  $p(\text{O}_2)=150$  mTorr. Thus, the changes in the observed morphology of YBCO films by  $p(\text{O}_2)$  are qualitatively described by the changes in the nucleation rates of the *c* axis and the [103,013] grains through the variations in  $\Delta G^*$  for the nucleus.

There is another possibility for the increasing tendency for the nucleation of [103,013]-oriented platelets with increasing  $p(\text{O}_2)$ , as shown in Fig. 2. This is the possibility that the interfacial energy  $\sigma_{(103)}$  is decreased with increasing  $p(\text{O}_2)$ , since  $\text{CeO}_2$  is known to be reduced under low  $p(\text{O}_2)$ . When  $\text{CeO}_2$  is reduced to  $\text{CeO}_{1.5}$ , its parameter increases from  $\sim 0.541$  to  $\sim 0.560$  nm.<sup>24</sup> The length of the one side of the YBCO's (103,013) planes is  $a_{(103)}=0.552$  nm. Thus, there is some value of  $p(\text{O}_2)$  at which the [103,013] nuclei fit well with the substrate. However, the increased tendency to form [103,013] platelets in this study was observed for higher  $p(\text{O}_2)$  values and not for the lower ones. Thus, it is unlikely that the observed trend in the microstructural changes as a function of  $p(\text{O}_2)$  is due to the reduction of the interfacial energy  $\sigma_{(103)}$  by high  $p(\text{O}_2)$  values.

In Fig. 1, the peak value of  $J_c$  for 4- $\mu\text{m}$ -thick films was reached at a lower  $p(\text{O}_2)$  than that for 3- $\mu\text{m}$ -thick films. As pointed out previously, when the precursor thickness increased sufficiently, we need to take into account the changes

in the nucleation barrier  $\Delta G^*$  due to the changes in  $p(\text{HF})$  at the nucleation sites.<sup>10</sup> In thick films, the first term in Eq. (5),  $\delta\mu_{\text{HF}}$ , is approximately given by<sup>10</sup>

$$\delta\mu_{\text{HF}} \approx -4kT \left( \frac{a}{W} + \frac{dD_g}{WD_s} \right) \quad (6)$$

for  $d \ll a$ . Here  $a$  is the average internuclei separation,  $d$  is the precursor thickness,  $W$  is the HF diffusion length in the gas phase, and  $D_s$  and  $D_g$  are the diffusivities of HF in the precursor solid and the process gas, correspondingly. In this analysis we assumed that  $\delta\mu_{\text{HF}}$  is determined by  $p(\text{HF})$  gradients which arise by HF diffusion through the solid precursor and then through the processing gaseous atmosphere. Then, the fact that the optimum  $p(\text{O}_2)$  for high- $J_c$  YBCO films is not a universal value with respect to the thickness of the precursor films simply follows from Eq. (6). When  $d$  is increased from 3 to 4  $\mu\text{m}$ , the absolute magnitude of  $\delta\mu_{\text{HF}}$  increases, and hence both of  $\Delta G^*_{(103)}$  and  $\Delta G^*_{(001)}$  decrease, and this results in the increased nucleation rates for both types of the grains. Thus, the maximum value of  $J_c$  was achieved at a lower  $p(\text{O}_2)$ .

The increased sharpness of the  $J_c$  peak with  $p(\text{O}_2)$  with the lowered  $p(\text{O}_2)$  for the maximum  $J_c$  in thicker films, however, has an important negative implication. This is the increased difficulty of making high- $J_c$  YBCO films, since  $p(\text{O}_2)$  has to be controlled very precisely. This narrow peak is due to the fact that the lowest  $p(\text{O}_2)$  for the growth of YBCO is limited by the decomposition line of YBCO in the  $p(\text{O}_2)$  vs  $1/T$  phase diagram. For example, at  $T=735$  °C,  $p(\text{O}_2)$  for the decomposition is  $\sim 40$  mTorr according to the processing phase diagram.<sup>15,25</sup> One possible way to lower the accessible  $p(\text{O}_2)$  level is to lower the reaction temperature. However, this slows the growth rates considerably, and it was difficult to achieve consistency in the values of  $J_c$ . Another possibility is to lower  $p(\text{H}_2\text{O})$  and the total processing pressure,<sup>11,15</sup> thus keeping the growth rates similar to that which was used here. This will be investigated in the future.

The above argument, which is based on  $\Delta G^*$  changes due to the  $p(\text{O}_2)$  variations, cannot account for the  $J_c$  degradation at low growth rates, 0.2 nm/s, of YBCO in Fig. 1. There are two possible causes for this, and both of them are related to the interaction of  $\text{CeO}_2$  and a component of the precursor, Ba, to form  $\text{BaCeO}_3$ . The first comes from our previous observation of the interface at the early stages of the reaction by transmission electron microscopy.<sup>19</sup> In this study, 1- $\mu\text{m}$ -thick YBCO was formed at a growth rate of  $\sim 0.1$  nm/s from the precursor on  $\text{CeO}_2$ -buffered single-crystalline  $\text{LaAlO}_3$ , and a significant incubation time for the nucleation of YBCO was observed. For example, there was no sign of interaction between the precursor and  $\text{CeO}_2$  after 10 min at the temperature. After 25 min, however, the formation of an amorphous layer was observed at the interface. This consisted of Ce, Ba, and O, and was likely to be a liquid at the reaction temperature. Upon further heat treatment, some  $\text{CeBaO}_3$  islands along with YBCO layers were found at the interface. The formation of the liquid, as well as  $\text{CeBaO}_3$ , was thought to be detrimental to the nucleation of the [001]-oriented grains of YBCO. Thus, faster growth rates in this

experiment possibly assisted the shortening of the incubation time and the nucleation of the [001] nuclei before the formation of the liquid and CeBaO<sub>3</sub>.

The other possibility is related to the kinetics of the nucleation process. As mentioned above, a nucleus forms when its size exceeds the critical size  $r^*$  in Eq. (2). However, at the same time, there a number of embryos, which do not reach the critical size. These dissolve and new ones are formed again. When there is very little or no interaction between the precursor components and the substrate, the dissolution of these embryos is not likely to damage the nucleation sites. However, since there is a strong tendency for the reaction between Ba in the precursor and CeO<sub>2</sub>, there is a possibility for the favorable nucleation sites to have been damaged when the subcritical embryos were dissolved. Thus, both of these possible effects of the precursor/CeO<sub>2</sub> interaction may cause a reduction or elimination of the favorable nucleation sites when the growth rates are low. In other words, the interface energy  $\sigma$  and hence  $\Delta G^*$  are increased by these effects and a higher  $p(\text{O}_2)$  is required to nucleate the  $c$ -axis-as well as [103,013]-oriented YBCO. Thus, the peak in  $J_c$  was shifted to higher  $p(\text{O}_2)$  and this made it difficult to synthesize films free of the granularity and of the [103,013] grains. Hence, a significant reduction was observed for the overall values of  $J_c$  for these films compared with those for the YBCO films grown at high growth rates, as seen in Fig. 1.

## V. CONCLUSIONS

In conclusion, we have demonstrated the possibility of manufacturing thick (3 and 4  $\mu\text{m}$ ) YBCO films with critical-current densities  $J_{cw}$  as high as 80 A/mm on flexible tapes by a scalable *ex situ* processing technology. Achieving these high- $J_c$  values required the optimization of  $p(\text{O}_2)$ ,  $p(\text{H}_2\text{O})$ , and the total process-gas pressures. Also, it was shown that this optimization was related to variations in the barrier heights, the critical Gibbs free energies  $\Delta G^*$  for the nucleation of the  $c$  axis, and the [103,103]-oriented nuclei with the changes in oxygen partial pressures. In addition, the important fact, which made this synthesis of YBCO films possible, was the pretreatment of the precursor films at lower temperatures. This treatment appeared to make the films more permeable to the gases and allowed the growth of the  $c$ -axis nuclei possible at high growth rates.

## ACKNOWLEDGMENTS

The authors greatly appreciate the American Superconductor Corporation for their generosity in providing them

with a substantial length of their excellent metallic substrates for this experiment. Without their kind cooperation, this work would have never taken place. This manuscript has been authored by Brookhaven Science Associates, LLC under Contract No. DE-AC02-98CHI-886 with the U.S. Department of Energy.

<sup>1</sup>J. Daley (unpublished).

<sup>2</sup>S. R. Foltyn, P. Tiwar, R. C. Dye, M. Q. Le, and X. D. Wu, Appl. Phys. Lett. **63**, 1848 (1993); S. R. Foltyn, Q. X. Jia, P. N. Arendt, L. Kinder, Y. Fan, and J. F. Smith, *ibid.* **75**, 3692 (1999).

<sup>3</sup>F. Feenstra, T. G. Holesinger, and D. M. Feldmann (unpublished).

<sup>4</sup>A. Gurevich, e-print cond-mat/0207526.

<sup>5</sup>Q. X. Jia, S. R. Foltyn, P. N. Arendt, and J. F. Smith, Appl. Phys. Lett. **80**, 1601 (2002); also S. R. Foltyn *et al.*, reported  $I_c$  of 1400 A/cm by a similar approach (unpublished).

<sup>6</sup>R. Feenstra, A. A. Gapud, F. A. List, E. D. Specht, D. K. Christen, T. G. Holesinger, and D. M. Feldmann, IEEE Trans. Appl. Supercond. **15**, 2803 (2005).

<sup>7</sup>L. Wu, V. F. Solovyov, H. J. Wiesmann, Y. Zhu, and M. Suenaga, Appl. Phys. Lett. **80**, 419 (2002).

<sup>8</sup>V. F. Solovyov, H. J. Wiesmann, L. Wu, M. Suenaga, K. Venkataraman, and V. A. Maroni, Physica C **415**, 125 (2004).

<sup>9</sup>V. F. Solovyov, H. J. Wiesmann, L. Wu, Y. Zhu, M. Suenaga, D. P. Norton, and K. R. Marken, IEEE Trans. Appl. Supercond. **13**, 2474 (2003).

<sup>10</sup>V. F. Solovyov, H. Wiesmann, and M. Suenaga, Supercond. Sci. Technol. **18**, 239 (2005).

<sup>11</sup>V. F. Solovyov, H. J. Wiesmann, L. Wu, Y. Zhu, and M. Suenaga, IEEE Trans. Appl. Supercond. **11**, 2939 (2001).

<sup>12</sup>A. Ichinose, A. Kikuchi, K. Tachikawa, S. Akita, and K. Inoue, Supercond. Sci. Technol. **15**, 262 (2002).

<sup>13</sup>J. Yoo *et al.*, J. Mater. Res. **19**, 1281 (2004).

<sup>14</sup>J. Yoo *et al.*, Supercond. Sci. Technol. **17**, 1209 (2004).

<sup>15</sup>Y. Zhang, R. Feenstra, J. R. Thompson, A. A. Gapud, T. Aytug, P. M. Martin, and D. K. Christen, Supercond. Sci. Technol. **17**, 1154 (2004).

<sup>16</sup>V. F. Solovyov, H. J. Wiesmann, M. Suenaga, and R. Feenstra, Physica C **309**, 269 (1998).

<sup>17</sup>V. F. Solovyov, H. J. Wiesmann, L. Wu, Y. Zhu, and M. Suenaga, Appl. Phys. Lett. **74**, 1911 (2000).

<sup>18</sup>V. F. Solovyov, H. J. Wiesmann, and M. Suenaga, Physica C **352**, 14 (2001).

<sup>19</sup>L. Wu, Y. Zhu, V. F. Solovyov, H. J. Wiesmann, A. R. Moodenbaugh, R. L. Sabatini, and M. Suenaga, J. Mater. Res. **16**, 2869 (2001).

<sup>20</sup>*The Nucleation*, edited by A. C. Zettelemyer (Marcel Dekker, New York, 1969).

<sup>21</sup>J. Burke, *The Kinetics of Phase Transformations in Metals* (Pergamon, New York, 1965).

<sup>22</sup>W. G. Maffortt, *Handbook of Binary Phase Diagrams* (Gerium, Schenectady, NY, 1984); J. P. Neumann, T. Zhong, and Y. A. Chang, *Cu-O*, Handbook of Binary Phase Diagrams (Gerium, Schenectady, NY, 1984).

<sup>23</sup>J. D. Jorgensen, B. W. Veal, A. P. Paulikas, L. J. Nowicki, G. W. Crabtree, H. Claus, and W. K. Kwok, Phys. Rev. B **41**, 1863 (1990).

<sup>24</sup>L. Wu, H. J. Wiesmann, A. R. Moodenbaugh, R. F. Klie, Y. Zhu, D. O. Welch, and M. Suenaga, Phys. Rev. B **69**, 125415 (2004).

<sup>25</sup>R. Feensta, D. K. Christen, J. D. Budai, S. J. Pennycook, D. P. Norton, J. H. Lowndes, C. D. Klanbunde, and M. D. Galloway, in *Proceedings of Symposium A-1 on High Temperature Superconducting Films at the International Conference on Advance Materials*, Strasbury, France, 1991, edited by L. Corena (North-Holland, Amsterdam, The Netherlands), p. 331.